

The Thinning of Arctic Sea Ice, 1988–2003: Have We Passed a Tipping Point?

R. W. LINDSAY AND J. ZHANG

Polar Science Center, University of Washington, Seattle, Washington

(Manuscript received 2 December 2004, in final form 13 June 2005)

ABSTRACT

Recent observations of summer Arctic sea ice over the satellite era show that record or near-record lows for the ice extent occurred in the years 2002–05. To determine the physical processes contributing to these changes in the Arctic pack ice, model results from a regional coupled ice–ocean model have been analyzed. Since 1988 the thickness of the simulated basinwide ice thinned by 1.31 m or 43%. The thinning is greatest along the coast in the sector from the Chukchi Sea to the Beaufort Sea to Greenland.

It is hypothesized that the thinning since 1988 is due to preconditioning, a trigger, and positive feedbacks: 1) the fall, winter, and spring air temperatures over the Arctic Ocean have gradually increased over the last 50 yr, leading to reduced thickness of first-year ice at the start of summer; 2) a temporary shift, starting in 1989, of two principal climate indexes (the Arctic Oscillation and Pacific Decadal Oscillation) caused a flushing of some of the older, thicker ice out of the basin and an increase in the summer open water extent; and 3) the increasing amounts of summer open water allow for increasing absorption of solar radiation, which melts the ice, warms the water, and promotes creation of thinner first-year ice, ice that often entirely melts by the end of the subsequent summer.

Internal thermodynamic changes related to the positive ice–albedo feedback, not external forcing, dominate the thinning processes over the last 16 yr. This feedback continues to drive the thinning after the climate indexes return to near-normal conditions in the late 1990s. The late 1980s and early 1990s could be considered a tipping point during which the ice–ocean system began to enter a new era of thinning ice and increasing summer open water because of positive feedbacks. It remains to be seen if this era will persist or if a sustained cooling period can reverse the processes.

1. Introduction

Floating ice pack is a key component of the Arctic Ocean physical and biological systems. It controls the exchange of heat, water, momentum, and gases at the sea surface. Changes in the albedo of the surface brought on by changes in the ice cover over very large areas are a major factor in global climate change. Through its role as a transporter of freshwater, it modifies the static stability of the ocean in key areas where deep convection occurs. The sea ice also blocks the solar flux to the water and hence is a major control factor for primary productivity. It also acts as a support structure for organisms from phytoplankton to seals, walrus, and polar bears while limiting access to the surface for seals and whales. This component of the Arctic environment is changing rapidly.

The summer sea ice extent has been retreating in recent years. In the summer of 2002 record low levels of ice extent in the Arctic were observed (Serreze et al. 2003), the ice extents in the summers of 2003 and 2004 were almost as low (Stroeve et al. 2005), and the summer of 2005 shows another record low. This follows the very low ice extent in the western Arctic in the summer of 1998 (Maslanik et al. 1999). This downward trend in the ice extent has been documented by many authors (e.g., Gloersen and Campbell, 1991; Parkinson et al. 1999; Johannessen et al. 1999; Comiso 2002). The trend in the September ice extent for the period 1979–2004 is -7.7% per decade (Stroeve et al. 2005), a value twice as large as that reported for the shorter period 1979–95 (Serreze et al. 2000).

The ice in the central pack is also thinning. Based on submarine measurements, the ice draft is reported by Rothrock et al. (1999) to have thinned by 40% from the 1960s and 1970s to the 1990s. Rothrock et al. (2003) discuss the anomalously thin ice of the 1990s from both observational and modeling perspectives through the year 2000. The model (similar to that used here) agrees

Corresponding author address: Ronald W. Lindsay, Applied Physics Laboratory, University of Washington, 1913 NE 40th St., Seattle, WA 98105.
E-mail: lindsay@apl.washington.edu

well with observations averaged over entire cruises and shows a thinning of the ice from 1988 to 1996. Furthermore, they compared the outputs from eight different models with results published in the scientific literature and found that they all show a local thickness maximum in 1987 and mostly thinning since then. As shown here, in recent years the ice has continued to thin at a considerable rate.

The mean circulation of the ice is illustrated by model simulations of the mean winter and summer ice velocities, which include assimilation of ice velocity data as described in section 2 (Fig. 1). The winter circulation is dominated by the anticyclonic Beaufort gyre in the Pacific sector of the basin (see Fig. 2 for location names) and the transpolar drift stream, which transports ice out of the gyre and into Fram Strait. Fram Strait is the primary location for ice export from the basin. In the summer the circulation is much weaker

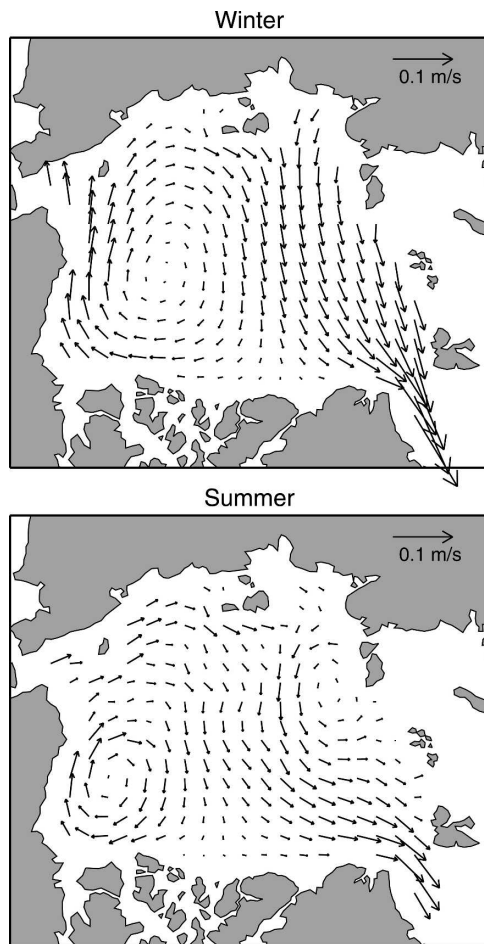


FIG. 1. Mean ice velocity for the period 1979–2003 in the winter (Oct–Apr) and summer (May–Sep). The anticyclonic Beaufort gyre is on the left and the Transpolar Drift Stream is in the center or on the right side of the Arctic Ocean.

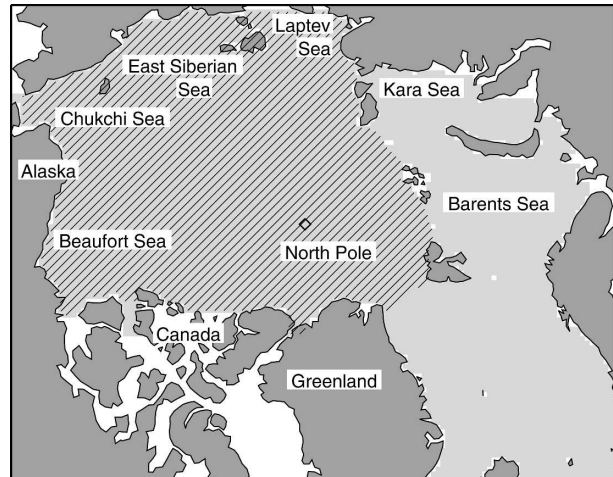


FIG. 2. The gray ocean region depicts the model domain. The cross-hatched area is the Arctic Ocean, the averaging region used for this study.

and the Beaufort gyre is smaller and is constrained mostly to the Beaufort Sea. The transpolar drift stream is much weaker and a small cyclonic gyre develops in the eastern part of the basin.

The drift of the ice is strongly dependent on the wind speed and direction (Thorndike and Colony 1982). For example, Thomas (1999) found that 56% of the variance of the ice velocity can be explained by a linear regression with the surface geostrophic wind. The geostrophic wind is determined by the surface sea level pressure (SLP) field. To summarize the large-scale temporal changes in the Northern Hemisphere SLP, Thompson and Wallace (1998) introduced the concept of the Arctic Oscillation (AO). The AO index is the time series of the first principal component of the Northern Hemisphere SLP. This component is associated with the first empirical orthogonal function (EOF) of SLP, which is an annular mode centered on the Arctic. In high AO periods the SLP is lower near the pole and the air temperature is higher in the Greenland–Iceland–Norwegian seas, the Barents Sea, and in eastern Siberia. The temperature is lower in northeastern Canada. The winter AO index changed to a strongly positive mode in 1989 and remained positive for 7 yr. The AO is closely related to another climate index, the North Atlantic Oscillation (NAO) (Hurrell 1995), which is largely determined by the strength of the Icelandic low.

The mean ice drift changes significantly with the AO (Rigor et al. 2002). When the AO index is high, the SLP Beaufort anticyclone is usually weaker and the Beaufort gyre ice circulation is usually weaker and displaced closer to the Alaskan coast. The transpolar drift stream

is also usually weaker; it is displaced nearer to the center of the basin and it swings more toward the north coast of Greenland before exiting the basin through Fram Strait. Zhang et al. (2000) find a strong dependence of the ice drift and modeled thickness patterns with the NAO. In another study Zhang et al. (2004) find that in global model simulations the heat inflow from the south over the Iceland–Scotland Ridge (ISR) is strongly correlated with the NAO. This heat flow has contributed to the continued thinning of Arctic sea ice since 1965. The ISR heat flow influences the ice thickness with a lag of 2–3 yr.

A second climate index that is important for Arctic sea ice is the Pacific Decadal Oscillation (PDO) (Man-tua et al. 1997). This index is based on the first EOF of the sea surface temperature in the North Pacific Ocean. The PDO is characterized by year-to-year persistence and shows positive/warm or negative/cool values that tend to prevail for 20–30-yr periods. However, within these periods there are several short-lived sign reversals, including 3- or 4-yr reversals from 1958 to 1961 and again from 1989 to 1991. The SLP in the North Pacific is correlated with the PDO and exhibits a stronger Aleutian low during the positive (warm) PDO phase. Here we show (section 6b) that the sea ice thickness in the Pacific sector of the Arctic Ocean, most notably from the east Siberian Sea to the pole, is well correlated with the winter PDO with a lag of 1 yr.

Köberle and Gerdes (2003) investigate the relative importance of the thermodynamic and dynamic forcings by holding either the monthly mean temperatures or the monthly mean winds to climatological values in model simulations. They find that the wind-forced and the thermally forced solutions for the total ice volume sum to give the total variation in the ice volume when both forcings are allowed interannual variability, indicating that the interaction of the wind-driven and the thermally driven changes is negligible. They also find that the variability of the ice volume due to the two forcings is similar but that specific episodes of ice thickening or thinning are created more by one or the other of the forcings.

With the same model described here (without data assimilation) Rothrock and Zhang (2005) examined the trend in the total hemispheric ice volume over the period 1948–99; two model simulations were performed: one with interannually varying winds and surface temperatures and one with no interannual variation of the temperature. Using the results of Köberle and Gerdes (2003), they find that the wind-forced component of the trend is very small and the temperature-forced component has a significant downward trend of -3% per decade.

Holloway and Sou (2002) argue that the decrease observed in the submarine ice draft record by Rothrock et al. (1999) is caused by aliased sampling of the spatial and temporal variability of the ice thickness. They suggest that the timing and cruise tracks of the submarines aliased a dominant mode of variability that consists of an oscillation between the Canadian sector and the central and Siberian sectors of the basin. However, Rothrock et al. (2003) report good agreement in the temporal changes in ice thickness between model simulations and the submarine observations and a basinwide thinning of the ice over the period 1987–97.

Here we argue that the recent considerable retreat of the summer ice extent and the continual rapid decline in the mean ice thickness is not a simple responses to either the thermodynamic forcing or the dynamic forcing, but an internal response of the system itself. This internal response was manifest when the slowly changing thermodynamic forcing created consistently thinner first-year ice at the start of the melt season and was triggered by a temporary change in the ice circulation patterns. The continual recent decline is not strongly dependent on either external forcing mode but is maintained and amplified by ice–albedo feedback processes within the ice–ocean system. The large changes that began in 1989 suggest that the system had reached a tipping point, a state of the system for which temporary changes in the external forcing (dynamics) created a large internal response that is no longer directly dependent on the external forcing and is not easily reversed. Of course conclusive evidence that the system did begin a long-term change in the late 1980s will require many additional years of observations.

The model and data assimilation methods are described briefly and comparisons with the observed ice draft measurements are discussed in section 2. In section 3 we introduce the model results and show how the ice reduction is partitioned between level and ridged ice categories. In section 4 the processes contributing to changes in the mean ice thickness over the 56-yr period are presented in order to provide a longer-term context in which to examine the recent thinning: thickness changes are partitioned into thermodynamic and dynamic effects, and the energy budget of the ice is examined. In section 5 an analysis of the recent considerable thinning in terms of the preconditioning, the trigger, and the response is presented. Further aspects of the recent thinning, including spatial characteristics, relationships to climate indexes, export at the Fram Strait, and recent air temperature trends are given in section 6. Finally, comments and conclusions are given in section 7.

2. Model description and data

We use a coupled ice–ocean model that has been used in a wide range of studies. The ice model is a multicategory ice thickness and enthalpy distribution model that consists of five main components: 1) a momentum equation that determines ice motion, 2) a viscous–plastic ice rheology with an elliptical yield curve that determines the relationship between ice deformation and internal stress, 3) a heat equation that determines ice temperature profile and ice growth or decay, 4) two ice thickness distribution equations for deformed and undeformed ice that conserve ice mass, and 5) an enthalpy distribution equation that conserves ice thermal energy. The first two components are described in detail by Hibler (1979). The ice momentum equation was solved using Zhang and Hibler's (1997) numerical model for ice dynamics. The heat equation was solved, over each category, using Winton's (2000) three-layer thermodynamic model, which divides the ice in each category into two layers of equal thickness beneath a layer of snow. The ice thickness distribution equations are described in detail by Flato and Hibler (1995). The ocean model is based on the Bryan–Cox model (Bryan 1969; Cox 1984) with an embedded mixed layer of Kraus and Turner (1967). Detailed information about the ocean model is found in Zhang et al. (1998) and about the enthalpy distribution model is in Zhang and Rothrock (2001).

The model domain (Fig. 2) covers the Arctic Ocean, the Barents and Kara Seas, and the Greenland–Iceland–Norwegian seas. It has a horizontal resolution of $40 \text{ km} \times 40 \text{ km}$, 21 ocean levels, and 12 thickness categories each for undeformed ice, ridged ice, ice enthalpy, and snow. The ice thickness categories, the model domain, and bottom topography can be found in Zhang et al. (2000). The model is forced with daily fields of sea level air pressure (SLP) and 2-m air temperature (T_{2m}) obtained from the National Centers for Environmental Prediction–National Center for Atmospheric Research (NCEP–NCAR) reanalysis (Kalnay et al. 1996) for the 56-yr period 1948–2003. The seasonally varying drag coefficient follows that of Overland and Colony (1994) with a minimum value of 0.97×10^{-3} in the winter and a maximum of 1.42×10^{-3} in the summer. The specific humidity and longwave and shortwave radiative fluxes are calculated following the method of Parkinson and Washington (1979) based on the SLP and T_{2m} fields. The cloud fractions used to compute the downwelling radiative fluxes only have seasonal variability and no spatial or interannual variability. Model input also includes river runoff and pre-

cipitation detailed in Hibler and Bryan (1987) and Zhang et al. (1998).

The ice concentration is assimilated from an ice concentration dataset originally created by Chapman and Walsh (1993). The dataset, the Global Sea Ice (GICE) dataset [a more recent version is the Hadley Centre Sea Ice and Sea Surface Temperature (HadISST) dataset; Rayner et al. (1996)], is obtained from the British Atmospheric Data Center. It consists of monthly averaged ice concentration on a 1° grid. In the satellite era (1979–2003) it is based largely on visible, infrared, and passive microwave measurements, and in the presatellite era on ship reports and climatology. For 2003 only we use the HadISST ice concentrations because the GICE dataset ends in 2002. We use data from 1948 to 2003 and linearly interpolate the monthly data to daily intervals. This interpolation method smoothes extreme values of the concentration, reduces the variability, and does not always maintain the reported monthly mean value (Taylor et al. 2000).

The assimilation procedure is outlined in Lindsay and Zhang (2005). Each day the model estimate C_{mod} is nudged to a revised estimate \hat{C}_{mod} with the relationship

$$\hat{C}_{\text{mod}} = C_{\text{mod}} + K(C_{\text{obs}} - C_{\text{mod}}), \quad (1)$$

and the gain (or weighting) function is

$$K = \frac{|C_{\text{obs}} - C_{\text{mod}}|^\alpha}{|C_{\text{obs}} - C_{\text{mod}}|^\alpha + R^2}, \quad (2)$$

where C_{obs} is the observed concentration, R^2 is the error variance of the observations, and the exponent $\alpha = 6$. This large exponent means that, only if the difference between the observations and the model is greater than about 0.5, are the observations heavily weighted, in effect only assimilating the ice extent. We use a fixed value of $R = 0.05$ that is consistent with the estimated errors of the GICE dataset. Changes in the thickness distribution were made to accommodate the change in the ice concentration in a manner that minimized changes in the ice mass by removing or adding ice to the thinnest ice classes.

Ice velocity measurements are assimilated with an optimal interpolation scheme outlined in Zhang et al. (2003). We use velocity measurements from both buoy-derived and Special Sensor Microwave Imager (SSM/I)-derived ice displacement data. The buoy velocities were obtained from the International Arctic Buoy Program (IABP), and SSM/I 85-GHz ice displacement measurements were provided by the Jet Propulsion Laboratory Polar Remote Sensing Group. The buoy velocities are 24-h averages and the SSM/I velocities are based on 2-day displacements. The passive microwave displacement estimates are based on a maximum

correlation method applied to sequential images of the ice cover. While the SSM/I daily velocity estimates have a substantially larger error standard deviation than the buoys (0.057 versus 0.007 m s^{-1}), their large number and excellent spatial coverage make them a valuable addition to our analysis.

Lindsay and Zhang (2005, manuscript submitted to *J. Atmos. Oceanic Technol.*, hereafter LIN05) also present comparisons between modeled and submarine measurements of ice draft; simulations were model-only or included assimilation of ice concentration (1948–2003) or assimilation of both ice concentration and velocity (1979–2003). The comparisons of the model and the observed ice draft are progressively improved with the assimilation of each variable. In the period 1987–97 the model-only simulation of the ice draft has a bias of -0.11 m and a correlation of $R = 0.51$ ($N = 835$ 50-km segments). With assimilation of ice concentration the bias is -0.30 m and the correlation is $R = 0.63$. When ice velocity is also assimilated, the bias is reduced to -0.02 m and the correlation increases to 0.70 ; the rms difference is 0.76 m . There is a strong spatial pattern in the bias of the model ice draft compared to the submarine ice draft, with the model showing ice too thick on the Pacific side of the basin and too thin on the Atlantic side. The spatial pattern of the model bias is puzzling because it persists even when ice velocity measurements are assimilated and hence the mean advective patterns are well estimated. This suggests that there may be some large-scale error in the model forcing or in the model physics.

Here we use the assimilation of ice concentration during the whole period of study and assimilation of ice velocity beginning in 1979 when ice velocity observations became abundant. Note that the assimilation of ice concentration and velocity did not greatly change the mean ice thickness simulations. The prominent maxima in 1966 and 1987 and the rapid decline in ice thickness since 1987 are present in all three simulations. The assimilation of ice velocity beginning in 1979 introduces an increase in the mean ice thickness of about 0.3 m over that of the assimilation of ice concentration alone; however our primary period of interest is 1988–2003, well after this change in the assimilation procedures. We use assimilation of both ice concentration and velocity to obtain a better representation of the details of the changes in the ice in this 16-yr period.

3. Model results: Changes in the mean thickness

In the model simulations one-third to one-half of the ice volume in the Arctic Basin is ridged ice and the rest is level ice. Figure 3 shows the time series of the mean ice thickness in the Arctic Ocean and the mean thick-

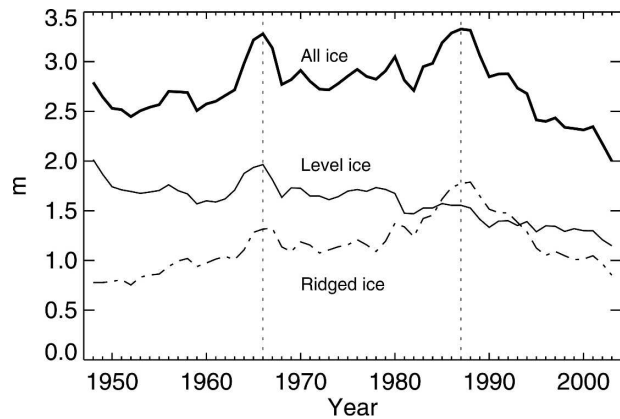


FIG. 3. Annual mean ice thickness (over the total area of the Arctic Ocean) of all ice, level ice, and ridged ice. The vertical lines indicate the times of the two principal maxima and are used in subsequent figures for reference.

ness (over the entire area) of level and ridged ice. Since 1988 the basinwide thickness has thinned by 1.31 m . During this period the volume of ridged ice has diminished more rapidly than that of the level ice. The level ice has been on a downward trend since 1966, but the ridged ice volume peaked in 1987 and 1988 and has fallen sharply since. The volume fraction of the ridged ice has fallen from 54% in 1988 to 46% in 2003. This result is consistent with the modeling studies of Makhtas et al. (2003) who also report that most of the decrease in sea ice thickness is caused by a decrease in ridged ice and an increase in the area of undeformed ice. Rothrock and Zhang (2005) report that a decline in the ice volume of level ice predominates. Rigor and Wallace (2004) explain the low summer sea ice extents of recent years as a delayed response to the high-index AO years of 1989–95 and to a change of the average age of the ice in the basin, a change that would also imply a decrease in the ridged ice volume.

The ice has thinned over almost all of the basin. At the time of the annual mean thickness maximum in 1987 and 1988 the mean ice thickness is at least 2.5 m over the entire central part of the basin, while in 2003 very little ice is greater than 2 m thick (Fig. 4). A narrow band of thick ice remains along the Canadian coast.

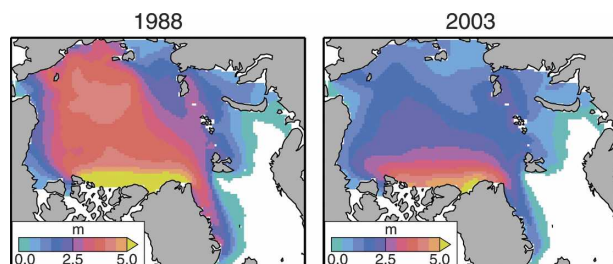


FIG. 4. Annual mean ice thickness for 1988 and 2003.

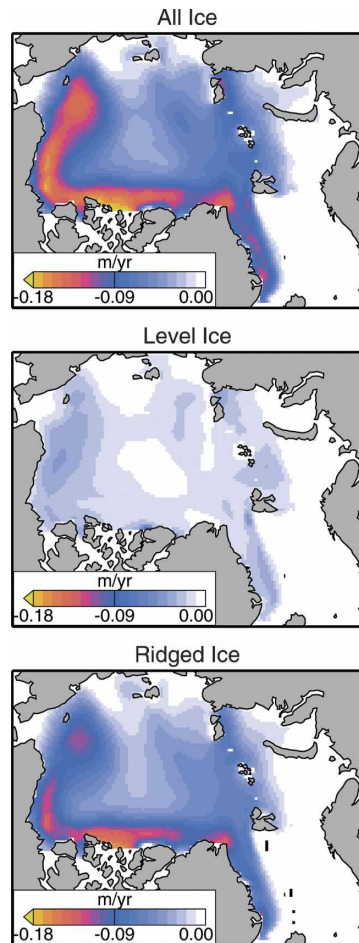


FIG. 5. Trend in the ice thickness for the 16-yr period 1988–2003 for all ice, level ice, and ridged ice.

Looking at just these 2 yr, the ice has thinned most in the east Siberian Sea, but the trend is quite different because it is derived from a linear fit of the ice thickness with time. For the 16 yr after 1988 the greatest trends are in the Beaufort Sea and along the Canadian coast (Fig. 5). There is a large reduction in the ridged-ice volume all along the Alaskan, Canadian, and Greenland coasts while the level-ice volume was reduced only slightly in the same period. The trend in the mean thickness is almost all due to the trend in ridged ice. Significance tests for the trend are not appropriate because the time interval analyzed is subjectively chosen to start with a maximum in the mean ice thickness and to specifically include a time when the trend is large. Clearly the trend in the basinwide mean thickness is greater in this 16-yr period than in any other 16-yr period in the 56-yr simulation (Fig. 3). Irrespective of the statistical significance of this trend, we are interested in the physical processes contributing to it.

The thinning trend for the 16 yr since 1988 is much

different from the trend for the full 56-yr simulation presented in LIN05 or Rothrock and Zhang (2005), which both show the thinning rate was greatest in the area north of the east Siberian and Laptev Seas and extended in a broad band to Fram Strait. Here, the more recent 16-yr period shows that the ice in the Siberian sector is generally thin first-year ice and the thinning trends are smaller in this sector than in the Canadian sector where ridged ice prevails. The maximum thinning rates are about -0.04 m yr^{-1} for the 56-yr period, while in the latest 16-yr period the maximum rates are 3 times as high, about -0.12 m yr^{-1} .

The model has 12 ice thickness bins that determine the ice thickness distribution. Comparisons of the thickness distributions for the whole Arctic Ocean for 1987 and 2003 show considerable changes. The mode is the bin with the largest area fraction. In May, at the start of the melt season, the mode is reduced by half, from 1.5 to 0.7 m. The ice is more concentrated in the thin bins: 22% more of the area is covered by ice less than 2 m thick. These simulations are supported by observations. Yu et al. (2004) report that observations of ice draft from submarines over the periods 1958–70 (a period of relatively thick ice) and 1993–97 (a period of rapidly thinning ice) also show a substantial loss of ice thicker than 2 m and increases in the amount of ice in the 1–2-m range. As reported here, they find the area fraction loss is greatest for the thickest ice categories.

Bitz and Roe (2004) argue that any change in the external forcing that thins the ice independent of its thickness causes the annual mean thickness of the thick ice to diminish more than that of the thin ice because of thermodynamic effects. For example, if the net energy flux to the ice increases, the anomalous increase in melt of thick and thin ice are comparable (as long as the thin ice does not melt away entirely), but thin ice responds by growing anomalously much faster in the winter. Hence, we would expect thicker ridged ice to diminish faster than thinner level ice under an increase in the net energy flux or, as explained by Bitz and Roe (2004), if ice divergence increases uniformly for all ice thicknesses.

4. Processes contributing to ice thickness change

a. Advection and thermodynamic growth

Changes in the mean ice thickness at each grid cell can be partitioned into two components: one due to the net advection and one due to thermodynamics. The net advection, or mass-flux convergence, is

$$\Delta \bar{h}_{\text{adv}} = - \int_t^{t+\Delta t} \nabla \cdot \bar{h} \mathbf{u} \, dt, \quad (3)$$

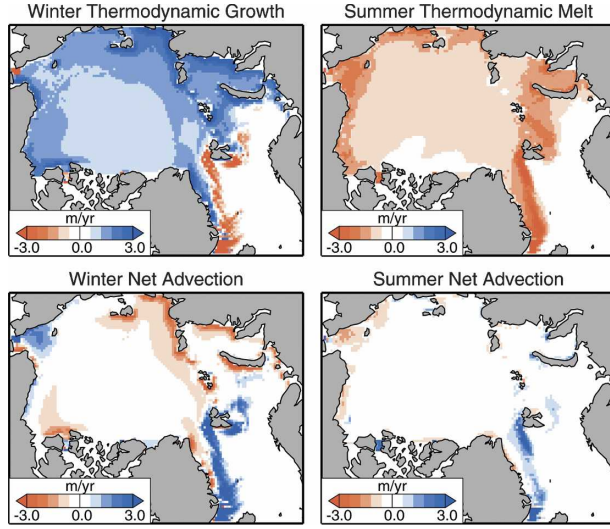


FIG. 6. Mean annual thickness changes due to thermodynamic growth or melt and net advection per year for winter (Oct–Apr) and summer (May–Sep) for the 56-yr period 1948–2003.

where \mathbf{u} is the vector velocity, \bar{h} is the mean ice thickness, and Δt is the time interval. The thermodynamic growth or melt is

$$\Delta \bar{h}_{\text{tdg}} = - \int_t^{t+\Delta t} \sum_{i=1}^{n_{\text{bins}}} [g(h_i)f(h_i) + \phi(h_i)] dt, \quad (4)$$

where the summation is over the thickness bins and $g(h)$ is the thickness distribution, $f(h)$ is the thermodynamic growth rate, and $\phi(h)$ is the lateral melt rate. The net thickness change over the interval is then

$$\Delta h = \Delta h_{\text{adv}} + \Delta h_{\text{tdg}}. \quad (5)$$

These terms of the ice mass balance have significant spatial and seasonal variability, as might be expected. Figure 6 shows the mean annual change in the thickness due to each of the two terms for the winter and summer seasons from the 56-yr simulation. There is net growth of 1 m or more over much of the basin in the winter and a lesser amount of melt in the summer. The net advection is quite small but slightly negative over most of the central part of the basin due to a small net divergence, divergence accommodated by the export of ice through Fram Strait. The region of greatest winter growth is in the Laptev Sea and in portions of the Kara and Barents Seas where more than 3 m of ice grows each winter. These are locations where there is often significant offshore flow and the continual creation of shore polynyas. Because of the winter offshore flow, the western Laptev is also a region of net advective loss in the winter but not in the summer when the winds are more variable. The eastern edge of the East Greenland Cur-

rent exhibits strong advective gain in both winter and summer, as well as strong melt in both seasons. Another region of strong advective gain in the winter is in the Chukchi Sea, where the anticyclonic Beaufort gyre brings thicker ice into the shelf region. Similarly, an advective loss is seen in the eastern Beaufort Sea where the gyre is pulling thick ice away from the coast.

These terms also show significant interannual variability. The annual total thermodynamic growth and net export, averaged over the Arctic Ocean (Figs. 7a and 7b), show the average winter growth is 1.30 m yr^{-1} and the average summer melt is -0.91 m yr^{-1} . The net advection is nearly zero in the summer and negative in the winter, averaging -0.41 m yr^{-1} . This term represents the net export of ice from the basin. The average thinning rate due to both processes over the entire 56-yr period is -0.02 m yr^{-1} .

The net change in the ice thickness is determined by the difference in the cumulative effect of large terms. Over the 56 yr of simulation, the thermodynamic winter growth totals 73 m of ice. This is balanced by summer melt and net advection to produce a net change of just -0.79 m (Fig. 3). So how, when, and where is the net change produced? To determine the integrative effect of anomalous periods of thickness change contributed by each of these terms we compute the cumulative anomaly from the mean (Figs. 7c and 7d). This type of plot simply shows periods of abnormal growth or melt when one of the terms is contributing more or less than normal to the change of the ice thickness. When the line is sloping upward (positive anomalies), the term is contributing to thickening of the ice more than average (either through more growth, less melt, or less advective loss than average) and, when the line is sloping down, it is contributing to thinning of the ice more than average (either through less growth, more melt, or more advective loss than average). By definition these plots must begin and end at zero. A consistent upward trend in one of the terms will appear as first a downward-sloping line (the anomalies are negative) and then an upward-sloping line (the anomalies are positive).

The sum of the annual lines in the cumulative plots reproduces the shape of the mean ice thickness line in Fig. 3 without the long-term 56-yr trend. The summer melt anomalies represent the largest contribution to the cumulative interannual variability of the thickness changes. There is a sharp decrease in the summer melt (upward-trending line) in the early 1960s contributing to the 1966 ice thickness maximum. The summer melt is generally less than average until 1987. The cumulative effect amounts to 2.5 m. After 1988 the melt is generally greater than average (downward-trending line). The

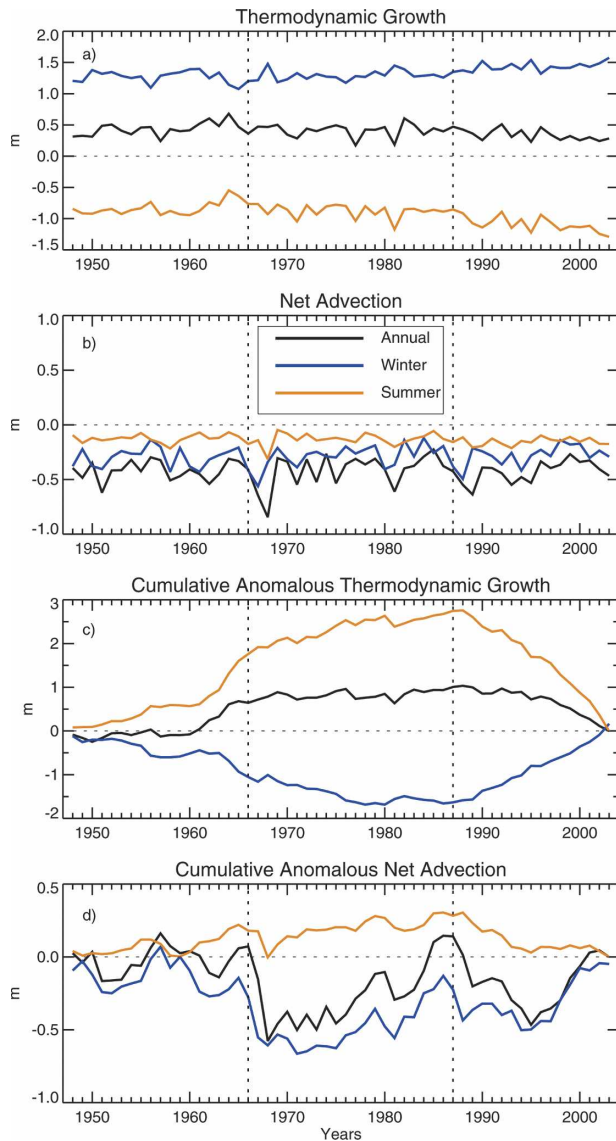


FIG. 7. Annual, winter (Oct–Apr), and summer (May–Sep) time series of the thermodynamic growth and net advection averaged over the Arctic Ocean. The top two panels show the yearly net thickness changes; the bottom two show the cumulative effect of anomalies from the mean for each parameter. Note the changes of scales. The lines for all of the panels are defined in the second panel.

winter freezing rates mirror, to a certain extent, the summer melt anomalies because when there is high summer melt and increased thin ice or open water the ice production rate in these regions in the subsequent winter is much larger. The net anomalous thermodynamic growth (black curve in Fig. 7c) leads to a thickening in the early 1960s and then little change until mid 1990s when the net change produces a thinning of the ice of about 1 m in the final few years of the study period.

The net effects of anomalies in advection are smaller than the anomalies in the thermodynamic terms and do not exceed 1 m (Figs. 7c and 7d). There is, however, a period of less-than-average winter advective loss (upward-sloping line) before the two maxima in 1966 and 1987 and more-than-average advective loss (downward-sloping line) after each one.

b. Surface heat balance

We can determine from the model simulations which components of the surface energy balance are responsible for changes in the thermodynamic growth. Consider the energy balance of a slab of ice. The fluxes of energy (positive if directed toward the ice) are the shortwave and longwave net radiation, F_{sw} and F_{lw} ; the sensible heat flux, F_s ; the latent heat flux, F_q ; and the conductive heat flux at the bottom of the ice, F_b . The balance is then expressed as a sum of the negative of the fluxes at the top and bottom surfaces plus the thermal energy stored in the ice, S , which is equal to the latent heat released in thermodynamic growth of the ice (or absorbed in melt if negative), F_{tdg} :

$$F_{tdg} = S - F_{sw} - F_{lw} - F_s - F_q - F_b. \quad (6)$$

For the annual mean we can assume the storage term S is zero. Figure 8 shows the mean annual values for each of the five source terms on the right expressed in equivalent meters of ice (after dividing by the latent heat of fusion for ice). The net solar flux is sufficient to melt 3 m of ice per year, but it is balanced by net

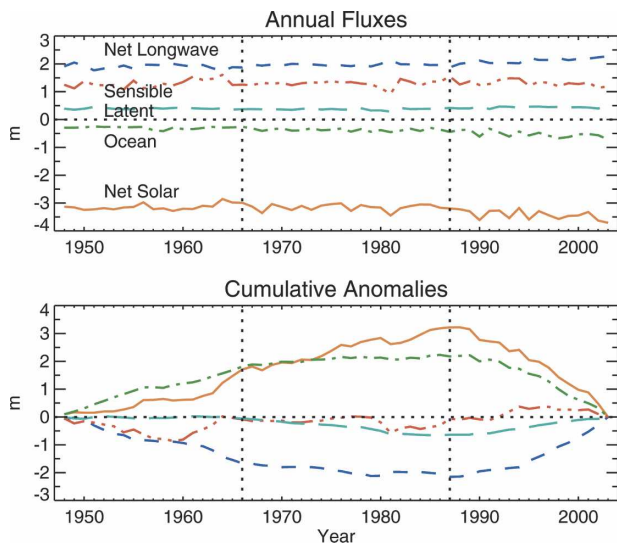


FIG. 8. (top) Annual mean net shortwave, net longwave, ocean, sensible, and latent heat fluxes expressed in terms of ice growth and (bottom) the cumulative anomalies of each. The fluxes are averaged over the Arctic Ocean.

longwave flux of about 2 m yr^{-1} , sensible heat flux of 1 m yr^{-1} , latent heat flux of 0.5 m yr^{-1} , and ocean flux of -0.5 m yr^{-1} . The cumulative anomalies of the terms are also shown. The radiative and ocean fluxes show the pattern of a consistent trend: the shortwave to increasing melt, the longwave to increasing growth, and the ocean flux to increasing melt. Each of these trends shows a change of sign in the anomalies near 1988, the year the precipitous drop in mean ice thickness began. The sensible and latent heat fluxes show no such trend and show no large change in the most recent 16 yr.

5. Analysis of the recent thinning

a. The preconditioning: Warming winter air temperature

The winter surface air temperature over the Arctic Ocean as represented in the NCEP–NCAR reanalysis has gradually warmed more than 3.5°C over the 56-yr simulation period. The time series of the basinwide-averaged 2-m air temperature for the four seasons is shown in Fig. 9. The 1948–2003 trends are winter: 0.63° , spring: 0.31° , summer: 0.03° , and fall: $0.54^\circ\text{C decade}^{-1}$. Of these only the summer trend is not significant at the 95% level. The trends in the reanalysis air temperatures need to be regarded with caution because of the changing set of observations available to the reanalysis effort (Kalnay et al. 1996); however, a number of other datasets also show warming in the winter and spring. Serreze et al. (2000) report that the annual mean air temperature from surface observations increased over virtually all coastal areas for the 30-yr period 1966–95 with trends locally greater than $0.5^\circ\text{C decade}^{-1}$. The warming has been greatest in the winter and spring seasons. Rigor et al. (2000) report that the air tempera-

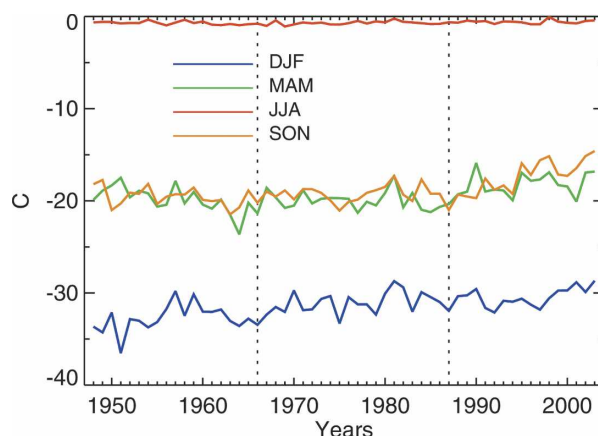


FIG. 9. Mean seasonal 2-m air temperatures from the NCEP–NCAR reanalysis averaged over the Arctic Ocean.

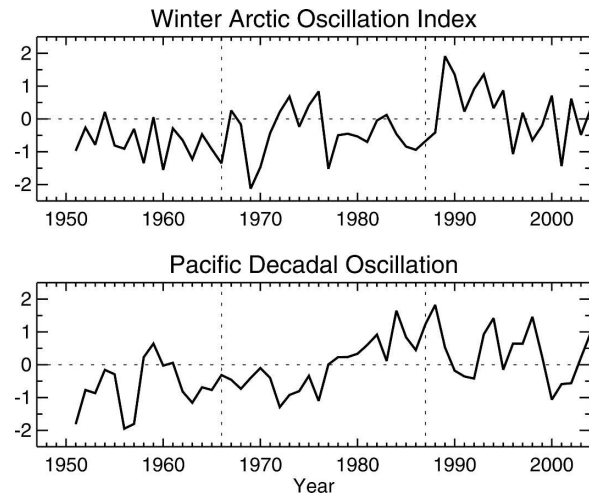


FIG. 10. Time series of the winter average (Nov–Mar) for (top) the Arctic Oscillation index and (bottom) the Pacific Decadal index. Both are in units of standard deviation.

ture from buoy observations in the 19-yr period 1979–97 over the Arctic Ocean has increased in the winter at a rate of $+1^\circ\text{C decade}^{-1}$ in the eastern Arctic Ocean and decreased $-1^\circ\text{C decade}^{-1}$ in the western portion of the basin, but during spring the air temperature has increased over virtually the entire basin and has increased at a rate of $2^\circ\text{C decade}^{-1}$ in the eastern Arctic Ocean. The effect of this warming on the level ice thickness is reflected in the annual mean level ice thickness (Fig. 3) where a decreasing long-term trend is evident.

The long-term thinning of the ice due to thermodynamic processes is also shown in the modeling study of Rothrock and Zhang (2005) who find that the downward trend in the total hemispheric ice volume over the period 1948–99 is primarily due to thermodynamic processes by comparing runs with and without interannual variation of the air temperature fields, a result substantiated by Köberle and Gerdes (2003) who find that since the mid-1960s thermal forcing has contributed more to the decline in the mean ice volume than dynamic forcing.

b. The trigger: Changes in climate indexes

Figure 10 shows the time series of the winter-averaged AO and PDO indexes. After the mean ice thickness maximum in 1987, the AO shifts from a negative phase to a 7-yr-long positive phase in the winter of 1989, while the PDO shifts from a 9-yr-long positive phase to a 3-yr-long negative one. This coincident shift in phase is not seen to the same extent in the rest of the record and is quite distinct from what happens after the 1966 maximum in the mean ice thickness. The shift in

the climate indexes caused a shift in the location and strength of the Beaufort gyre and the creation of large extents of summer open water, beginning in 1990. Figure 11 shows the September open water fraction in the Arctic Ocean from the GICE dataset. The mean open water over the Arctic Ocean has greatly increased in the last 16 yr compared to the previous 38 yr, but the trend is frequently broken by years with reduced open water.

The two prominent maxima in the ice thickness time series (Fig. 5) are characterized by different processes. Before 1966 there is a sharp decrease in the summer melt rate and a modest decrease in the net advective loss leading to an increase in the thickness (Fig. 7). After 1966 a sharp increase in the advective loss and little change in the thermodynamic terms lead to a sharp drop in the thickness. The simulations of Köberle and Gerdes (2003) also show that the maximum in the mid 1960s was mostly thermally forced and that there was a sharp decrease in the thickness just after the maximum caused by their wind-driven simulation.

Before the 1987 maximum there is little change in the sum of the thermodynamic terms (Fig. 7); there is, however, a decrease in the advective loss before the maximum and then a sharp increase after. This increase in the advective loss of ice is the trigger for beginning the sustained loss of ice in the Arctic Ocean. The simulated loss is consistent with the surge of old ice lost from the ocean during this time period reported by Rigor and Wallace (2004) and Fowler et al. (2004) and also with the model results of Makshtas et al. (2003), who show that the recent thinning coincides with a decrease in the concentration of ridged ice.

c. The feedback: Ice–albedo interactions

The ice–albedo feedback is a positive feedback in the ice–ocean system in which reduced ice extent leads to a lower mean albedo and increased absorption of solar energy. This, in turn, leads to more ice melt and reduced ice extent. It also functions for thin ice, which has a lower albedo than thick ice, so that thin ice absorbs more solar flux and hence melts more quickly than thick ice. This feedback can locally be highly nonlinear since the absorbed solar flux is a nonlinear function of the ice thickness.

The first year of extensive summer open water is 1990, after the strong advective loss of ice in 1989 (Fig. 11). For both the 1966 maximum and the 1987 maximum, the open water expanded greatly about 3 yr after the maximum and after the main pulse of advective loss occurred. The figure shows the remarkable increase in the late summer open water extent in the 1990s and shows that the last year of the record, 2003, had the

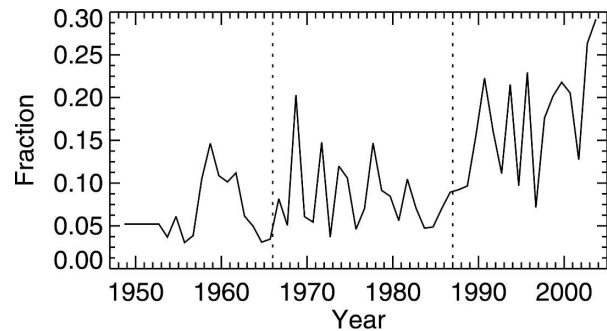


FIG. 11. September open water extent from the GICE dataset as a fraction of the area of the Arctic Ocean. The open water extent is the area with ice concentration less than 0.15.

greatest open water extent, measured as a fraction of the area of the Arctic Ocean, in the entire record. This record year is different from the 2002 record minimum ice extent reported by Serreze et al. (2003) because here only the Arctic Ocean ice extent is accounted for while they included the Canadian Archipelago and the Barents and Kara Seas as well.

Since 1988 the largest net change in the surface fluxes compared to the mean values, amounting to the equivalent of about 3 m of ice loss, is that due to the net solar flux (Fig. 8). This loss is partially compensated by a change in net longwave flux equivalent to about 2 m of ice gain, a large amount because of the heat lost from the warmer open water or thin ice surfaces. The loss of ice during this period due to ocean heat flux is about 2-m ice equivalent. Some of this ocean heat is from the solar heat absorbed by open water. Notably the change in ice thickness due to changes in the turbulent sensible and latent heat terms is relatively small. These fluxes are largely determined by the air temperature (relative to the ocean temperature), so the recent changes in the mean ice thickness are not primarily due to recent changes in the surface air temperature.

The increased net solar flux in the simulations can only arise from changes in the model albedo because the cloud fraction in the model, and hence the estimate of the downwelling solar flux, has no interannual variability. These simulations isolate the ice–albedo feedback from possible real changes in the downwelling solar flux. The downwelling solar fluxes may not, in fact, be constant. Schweiger (2004) discusses the seasonal trends in the cloud fraction observed by both the Advanced Very High Resolution Radiometer (AVHRR) and the Television and Infrared Observation Satellite (TIROS) Operational Vertical Sounder (TOVS) satellite systems. He finds a strong downward trend since 1980 in the TOVS-based winter cloudiness over oceans north of 60°N and an upward trend in the spring cloudiness. This is consistent with the AVHRR-based esti-

mates of Wang and Key (2003) but not with the AVHRR-based estimates of Comiso (2003). A winter decrease in the cloud fraction would decrease the downwelling longwave flux, resulting in more ice growth. Curry and Ebert (1992) find in a modeling study that over ice in the Arctic Ocean, the cloud radiative forcing is positive in all seasons except for mid-summer and that clouds have a net warming effect on the surface, so presumably the increased cloudiness in the spring would reduce ice growth. The albedo changes in the model are consistent with satellite-based observations of decreasing trends in the basinwide mean albedo (Comiso 2001; Laine 2004) and with the observations from passive microwave sensors of the decreasing basinwide summer ice extent.

The responses of the longwave fluxes in recent years can be understood as responses of the system to changes in the ice thickness and concentration. Increased open water and thin-ice fractions result in increased surface temperatures in the cold seasons. These increased surface temperatures allow increased longwave emissions to the atmosphere. The ocean flux increases in response to the recent changes in albedo as more radiation is absorbed by the water, warming it and providing more heat for ice melt.

6. Further characteristics of the thinning

a. Spatial patterns

What is the spatial distribution of the processes contributing to the recent (1988–2003) thinning? Figure 12 represents the trends of the net thermodynamic growth or melt and the net ice advection. The trend in the mean ice thickness for the same period (Fig. 5) is made of the sum of these two fields (note that they have different color scales). The net trend in the ice thickness is caused by different processes in different parts of the basin. In the Chukchi and Beaufort Seas there is a large increase in the net advection that is more than offset by an even larger increase in the net melt of ice. The large increase in advection is due, at least in part, to decreasing thick ice in this region and increasing net ice drift from the east in the Beaufort gyre. In contrast, the loss of ice in the region north of Canada and Greenland is caused primarily by increasing net advective loss, not by increasing melt. The loss of ice in Fram Strait and north of Svalbard is caused by thermodynamic processes dominating over advective processes. The net advection is increasing in this area because the region of strong thickness gradient has moved north. Along the Siberian coast the increasing net advection has led to a loss of ice that is almost balanced by increasing

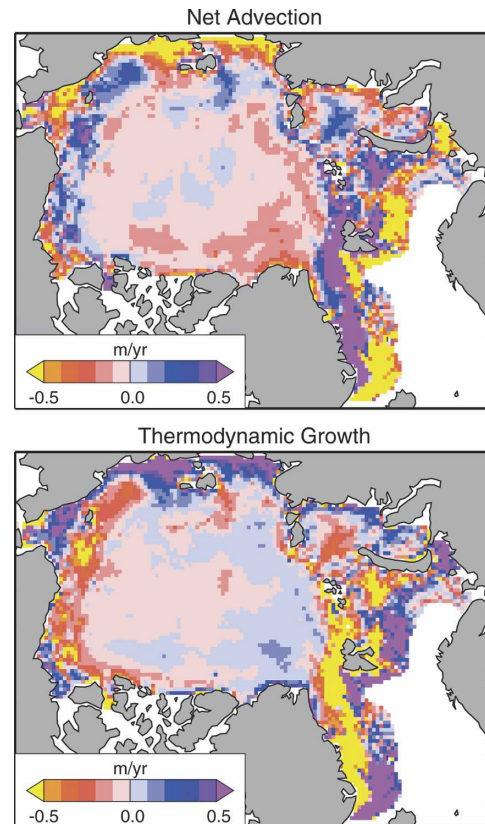


FIG. 12. Spatial patterns of the trends in the annual thermodynamic growth and net advection for the 16-yr period 1988–2003. The sum of these two fields gives the trend in the mean ice thickness seen in Fig. 5 for all ice.

thermodynamic growth and hence the trends in the ice thickness are small.

The map of thermodynamic growth trends may imply important ongoing changes in the salt flux at the ocean surface. Where there is decreasing net annual growth (usually through more melt) the salt flux is reduced and may become negative, while where there is increasing growth (through more freezing in open water or through less melt) the salt flux is increasing. The increasing growth rates along the Siberian coast and the decreasing rates in the Beaufort and Chukchi Seas may impact the ocean circulation on these shelves. The growth trends east of Greenland imply a shift farther north in the location of the freshwater released by the melting ice.

b. Climate indexes

The AO has a nearly basinwide effect on the ice thickness while the PDO is particularly important for the ice in the Siberian sector of the basin. Figure 13

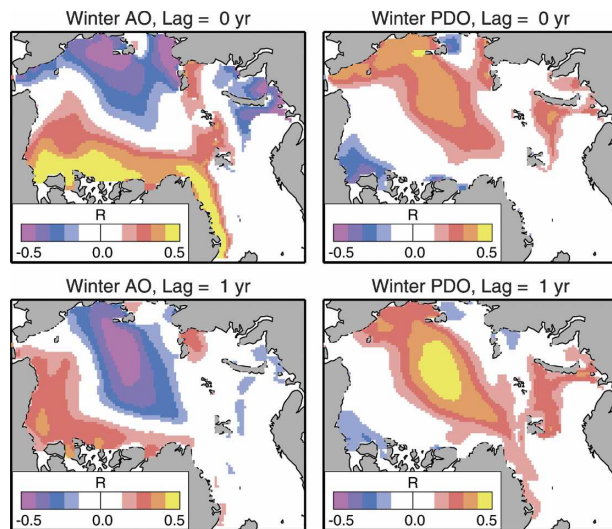


FIG. 13. Correlations of the annual mean ice thickness with the winter (Nov–Mar) AO and the PDO indexes for a lag of zero or 1 yr. The zero lag indicates the correlation of the ice thickness with the index for the winter ending in the same year, and the 1-yr lag the correlation with the index of the previous winter. Absolute correlations greater than 0.33 for the AO and greater than 0.40 for the PDO are significant at the 95% level.

shows the correlation of the two winter indices with the annual mean ice thickness for each location for the subsequent calendar year (lag 0) and for the year after (lag 1). The AO is positively correlated with the annual mean thickness along the Canadian coast and in Fram Strait and negatively correlated with the thickness in the east Siberian Sea. This is consistent with the findings of Rigor et al. (2002), who studied how the circulation of the ice is correlated with the AO and with changes in the geostrophic wind circulations in the basin. The correlations are smaller at a lag of 1 yr, but note how the region of most negative correlation has drifted along the northern side of the Beaufort gyre at about the rate of the mean annual drift.

The PDO is positively correlated with the mean thickness in a broad region extending from the east Siberian Sea to the North Pole and the correlation increases (and is at its maximum) at a lag of 1 yr. The positive PDO (warm phase) is associated with a stronger Aleutian low (Mantua et al. 1997) and a stronger SLP Beaufort anticyclone, which increases the strength of the Beaufort gyre and reduces the rate of advection of thick ice out of the east Siberian Sea. A negative PDO reduces the strength of the Beaufort gyre and increases the rate of advection out of the east Siberian Sea, as happened in the late 1980s and early 1990s.

The large change in the atmospheric circulation in 1989 was first indicated in a report by Walsh et al. (1996). They observed that the annual average sea level

pressure anomalies north of 70°N shifted to a strongly negative mode starting in 1989 and continuing through 1994. The impact of this shift on the ice circulation is described by Rigor and Wallace (2004).

Holloway and Sou (2002) report a sharp change in the first principal component of their model mean ice thickness in 1989, a shift that would indicate thinner ice in the Siberian and central sectors and thicker ice in the Canadian sector. This change in the modes of variability of the ice thickness in 1989 is also supported in an EOF analysis of the present model (LIN05). In this analysis it is the second and third principal components that shift in 1989. Both of these modes show cross-basin anticorrelations, which together are similar to the first EOF of Holloway and Sou. Proshutinsky and Johnson (1997) find that ice drift in a wind-driven model shows distinct cyclonic and anticyclonic regimes, each of which persists for 5–7 yr. Their analysis also shows that 1989 was a transition year when the circulation switched from anticyclonic (strong Beaufort gyre) to cyclonic (weak Beaufort gyre).

The change in the ice circulation is illustrated by Zhang et al. (2000), where they show the difference in the mean ice motion for the periods 1979–88 versus 1989–96. During the first period the Beaufort gyre is strong and is able to advect ice rapidly into the Chukchi Sea from the Beaufort Sea, while during the later period the gyre is weak and is located nearer the Alaskan coast. The export of thick ice through Fram Strait is increased in the later period. Our simulations show that in the period 1997–2003 the ice drift returned to more normal conditions, even as the thinning continued.

c. Export at Fram Strait

The initial loss of ice associated with the strong positive anomaly of the AO is coincident with larger-than-normal ice export rates at Fram Strait in 1988 and 1989. The simulated ice export at Fram Strait is shown in Fig. 14. The mean ice thickness at the strait reflects the basinwide mean thickness, showing a decline since 1989. The area transport rate, which averages 13% of the basin area per year, is about half as large in the summer as in the winter. The correspondence with the observed mean area flux determined by tracking the ice in passive-microwave images (Kwok et al. 2004) is quite good because similar observations of the ice velocity are assimilated. There is not a significant trend in the area flux or a large increase in the area flux in the period following either of the two principal maxima in the ice thickness. The volume flux has an annual average of 0.39 m of ice per year when averaged over the area of the Arctic Ocean. The correspondence with the Kwok et al. (2004) estimates, which are based on mea-

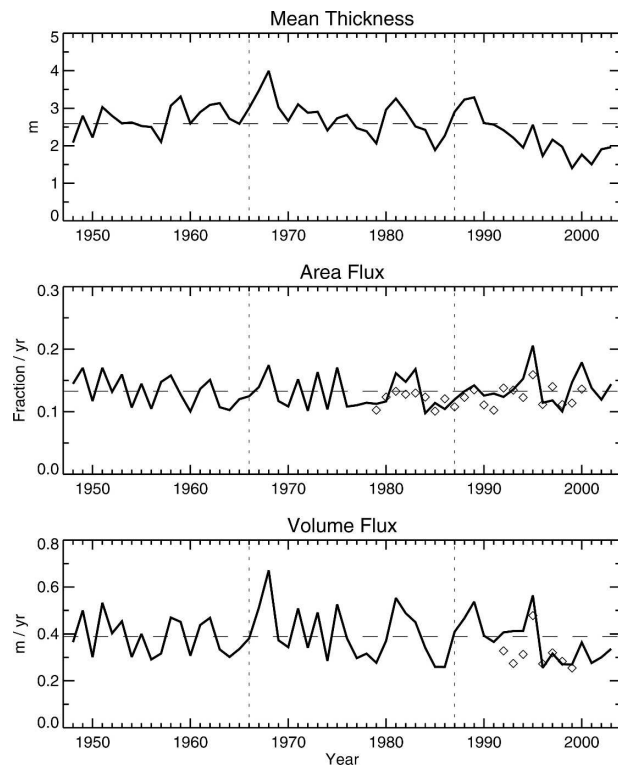


FIG. 14. Annual ice export at Fram Strait: mean ice thickness, ice area transport rate (expressed as fraction of the area of the Arctic Ocean per year), and the ice volume transport rate (expressed as ice thickness over the area of the Arctic Ocean). The dashed lines are the mean values and the symbols are the observed transport rates from Kwok et al. (2004).

measurements of the ice draft from moored upward-looking sonars, is also quite good. The volume transport is the product of the area transport and the mean thickness and, hence, shows greater variability than either of the two. The volume export at Fram Strait is similar to the net advection averaged over the basin (Figs. 6b and 14c, the signs are opposite), but there are two other passages in the model out of the Arctic Ocean that have a minor effect on the mass balance, one into the Barents Sea and one into the Kara Sea. The winter volume flux at Fram Strait is particularly large just after both of the two principal maxima, more because the mean thickness is large than because the area flux is large. This is because the origin of ice exiting the basin is more from north of Greenland, where the ice is thick, than from north of Svalbard, where it is thinner. The winter volume flux declines in the late 1990s because the mean thickness declines, not because there is a significant change in the area flux.

d. Recent air temperature changes

The annual mean rate of warming of the surface air temperature represented in the NCEP–NCAR reanalysis

dataset over the Arctic Ocean has increased, from $0.15^{\circ}\text{C decade}^{-1}$ (1948–87) to $1.17^{\circ}\text{C decade}^{-1}$ (1988–2003); only the later trend is significant at the 95% level. The rate of warming is greater in the last 16 yr in the fall than in winter or spring. Figure 15 shows maps of the seasonal trends in the 2-m air temperature in the 16-yr period 1988–2003. The warming over some locations in the Arctic Ocean in the fall is considerable and the warming persists into the winter and spring months in isolated areas. The mean trends over the Arctic Ocean are winter: 1.02° , spring: 0.62° , summer: 0.00° , and fall: $3.00^{\circ}\text{C decade}^{-1}$ (1988–2003). Of these, only the fall trend is significant at the 95% level. Much of the land area shows marked cooling during this period, particularly in the spring over western North America. The air temperature is a forcing for the ice–ocean model and is itself a result of the NCEP–NCAR atmospheric reanalysis model. The reanalysis model does not assimilate measured surface air temperatures but computes them as a diagnostic after assimilating various other atmospheric measurements, so these trends must be regarded with caution.

Trends in air temperature are notoriously dependent on the interval examined. The patterns of recent warming shown here are quite different from what Rigor et al. (2000) reports for the 19-yr period 1979–97, which included years before the ice maximum. They show the strongest warming in the spring. The fall warming noted here is consistent with simulations of climate

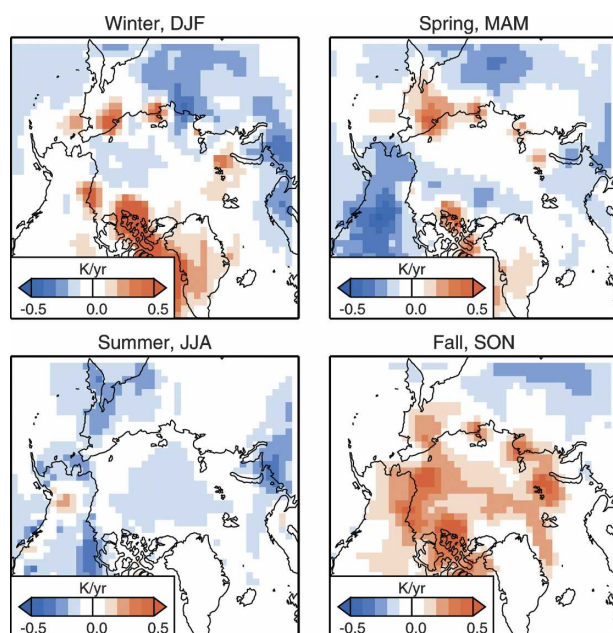


FIG. 15. Seasonal trends in the 2-m air temperature from the NCEP–NCAR reanalysis for the 16-yr period 1988–2003.

change in the Arctic performed by global climate models, which also show maximum warming over the Arctic Ocean in the fall under increased-greenhouse-gas scenarios (Moritz et al. 2002).

The recent, more rapid increase in the fall air temperature over the Arctic Ocean reinforces, and may be caused by, a thinning of the ice that is predominately driven by the ice–albedo feedback. The change in the ice thickness due to changes in the sensible and latent heat fluxes is negligible. The net longwave flux has contributed to a thickening of the ice in recent years, not a thinning that might be expected since the model estimate of the downwelling longwave flux increases with increasing surface air temperatures.

The increased melt in the summer is closely related to changes in the duration of the melt season. Belchansky et al. (2004) find that passive microwave–based estimates of the duration of the melt season were longer in the period 1989–2001 compared to 1979–88. The mean duration of the melt season was largest in 1989, just after the winter AO index was at its highest and near the beginning of the recent thinning. They find that the increase in the melt season length is greatest in the northern Chukchi Sea, near the area where there has been increased summer open water extent. They also find that despite recent declines in the winter AO index, the melt duration has not returned to the pre-1988 values nor have the spatial patterns in the melt duration returned to those seen in the 1979–88 low-index AO period.

7. Comments and conclusions

The results presented here are from model simulations and as such need to be regarded with some caution. Long-term trends in the model results are particularly difficult to assess for several reasons. First, the model physics or model resolution may not be adequate to properly reflect the long-term evolution of the ice–ocean system. Second, the climatological cloud cover assumed by the model does not reflect the true state of the system and may be a significant source of error for the downwelling radiative fluxes. Finally, the forcing fields of temperature and geostrophic wind may not be of sufficient accuracy to reflect trends in these parameters given that the mix of observations available to the reanalysis effort has changed significantly over the years. We feel, however, that short-term trends, such as those of the last 16 yr of the study period, are more accurately represented in the reanalysis model simulations because the observational base is more abundant and consistent during this period than in the presatellite era.

Since 1988 sea ice in the Arctic Ocean has thinned dramatically in model simulations. The thinning is a result of preconditioning, a trigger, and positive feedbacks. Here we report the following:

- Maxima in basinwide ice thickness occurred in 1966 and 1987 and the later maximum was followed by a large and consistent decrease in the mean thickness through 2003 (Fig. 3). The thinning rate is greatest in the Alaska–Canada–Greenland sector (Fig. 5). Observations from submarines are consistent with the simulated thinning for the period 1986–98 (Lindsay and Zhang 2005) and the amount of ridged ice has decreased considerably since 1987 while the volume of level ice has declined only slightly (Figs. 3 and 5). Both flushing of ridged ice from the basin and the preferential thinning of thick ice have led to this reduction in ridged ice.
- The basinwide average change in the thickness is usefully partitioned between winter and summer thermodynamic growth or melt and net advection. The largest source of variability is in the summer melt, which shows a consistent trend of increasing melt over the 56-yr study period and a marked increase in the melt trend in the last 16 yr (Fig. 7). Winter freezing rates follow the summer melt rates: when there is increased summer melt, there is increased winter ice production. Net advection averaged over the basin has not changed much over the study period but there was a spike in the volume export at Fram Strait just after the 1987 maximum and again in 1995 (Fig. 14). Since then, the volume export has diminished because the mean thickness crossing Fram Strait is less, not because the area transport is less.
- The winter air temperature over the Arctic Ocean has gradually warmed over the 56-yr period leading to a reduced equilibrium ice thickness (Fig. 9). In the last 16 yr the air temperature over the Arctic Ocean has changed most in the fall, when there is considerable warming (Fig. 15). We believe this recent fall warming can be attributed to the thinning ice cover, which allows more heat from the ocean to warm the air, the additional heat having been absorbed through open water in the summer.
- Two primary climate indices for the Arctic, the AO and the PDO, both changed in 1989 (Fig. 10). The high AO index in the late 1980s and early 1990s caused a flushing of some of the old, thick, ridged ice through Fram Strait. The AO and PDO indices have returned to near-normal values since the mid-1990s; yet the simulated thinning continues unabated.
- The reduced summer ice extent and summer ice concentrations have led to a considerable increase in the

absorbed solar flux and further reduction of the ice volume through the ice–albedo feedback mechanism (Fig. 8).

In summary, the thinning is due to 1) fall, winter, and spring air temperatures over the Arctic Ocean gradually increasing over the last 56 yr, leading to reduced thickness of first-year ice at the start of summer (the preconditioning); 2) a temporary shift, starting in 1989, of two principal climate indices causing a flushing of some of the older, thicker, ice out of the basin and an increase in the summer open water extent (the trigger); and 3) the recent increasing amounts of summer open water allows increased absorption of solar radiation, which melts the ice, warms the water, and promotes creation of thinner first-year ice, ice that then often entirely melts by the end of the subsequent summer (the feedback).

To answer the title question, we believe that 1989 does represent a tipping point for the Arctic ice–ocean system because the system had reached a state in which triggering events were able to initiate a process of continual rapid change even though the external forcings have changed little. Sea ice and ocean processes related to the positive ice–albedo feedback dominate the recent thinning processes. However, at this point we can only state the tipping point as a hypothesis. Further modeling studies may shed additional light on the nature of the changes seen in recent years, but proof that the late 1980s were a significant turning point for the ice–ocean system will only come with further observations of the system.

It is quite possible that the large changes initiated by the gradual winter warming and the atmospheric circulation anomalies of the early 1990s have forced the system into a new state in which very large extents of summer open water and winter first-year ice are the norm. The old regime may not be regained until there is either a prolonged cooling period or a prolonged period of very negative AO index and positive PDO index that can once again build the reservoir of thick ridged ice through strengthening the circulation of the Beaufort gyre. The gradually increasing winter air temperatures may reflect a global warming signal that will preclude a return to the old regime.

Acknowledgments. The NCEP–NCAR reanalysis data were obtained from the National Center for Atmospheric Research, the GICE and HadISST datasets were obtained from the British Atmospheric Data Center, the AO data are from the NOAA Climate Prediction Center, the PDO data are from N. Mantua, the buoy data are from the International Arctic Buoy Pro-

gram, and the passive microwave data are from the Polar Remote Sensing Group at the Jet Propulsion Laboratory. We gratefully acknowledge discussions with D. Rothrock, A. Schweiger, and M. Steele, and the very helpful comments of the reviewers. This work was supported by the NASA Cryospheric Sciences, Global Modeling and Analysis, and Radiation Sciences Programs; the NOAA Arctic Research Program; and the NSF Office of Polar Programs.

REFERENCES

- Belchansky, G. I., D. C. Douglas, and N. G. Platonov, 2004: Duration of the Arctic sea ice melt season: Regional and interannual variability, 1979–2001. *J. Climate*, **17**, 67–80.
- Bitz, C. M., and G. H. Roe, 2004: A mechanism for the high rate of sea ice thinning in the Arctic Ocean. *J. Climate*, **17**, 3622–3631.
- Bryan, K., 1969: A numerical method for the study of the circulation of the world oceans. *J. Comput. Phys.*, **4**, 347–376.
- Chapman, W. L., and J. E. Walsh, 1993: Recent variations of sea ice and air temperatures in high latitude. *Bull. Amer. Meteor. Soc.*, **74**, 33–47.
- Comiso, J. C., 2001: Satellite-observed variability and trend in sea ice extent, surface temperature, albedo, and clouds in the Arctic. *Ann. Glaciol.*, **33**, 457–473.
- , 2002: A rapidly declining perennial sea ice cover in the Arctic. *Geophys. Res. Lett.*, **29**, 1956, doi:10.1029/2002GL015650.
- , 2003: Warming trends in the Arctic from clear sky satellite observations. *J. Climate*, **16**, 3498–3510.
- Cox, M. D., 1984: A primitive equation, three-dimensional model of the oceans. GFDL Ocean Group Tech. Rep. 1, NOAA/Geophysical Fluid Dynamics Laboratory, Princeton, NJ, 143, pp.
- Curry, J. A., and E. E. Ebert, 1992: Annual cycle of radiation fluxes over the Arctic Ocean: Sensitivity to cloud optical properties. *J. Climate*, **5**, 1267–1280.
- Flato, G. M., and W. D. Hibler III, 1995: Ridging and strength in modeling the thickness distribution of Arctic sea ice. *J. Geophys. Res.*, **100**, 18 611–18 626.
- Fowler, C., W. J. Emery, and J. Maslanik, 2004: Satellite-derived evolution of Arctic sea ice age: October 1978 to March 2003. *IEEE Geosci. Remote Sens. Lett.*, **1**, 71–74.
- Gloersen, P., and W. J. Campbell, 1991: Recent variations in Arctic and Antarctic sea-ice covers. *Nature*, **352**, 33–36.
- Hibler, W. D., III, 1979: A dynamic thermodynamic sea ice model. *J. Phys. Oceanogr.*, **9**, 817–846.
- , and K. Bryan, 1987: A diagnostic ice–ocean model. *J. Phys. Oceanogr.*, **17**, 987–1015.
- Holloway, G., and T. Sou, 2002: Has Arctic sea ice rapidly thinned? *J. Climate*, **15**, 1691–1701.
- Hurrell, J. W., 1995: Decadal trends in the North Atlantic Oscillation: Regional temperatures and precipitation. *Science*, **269**, 676–679.
- Johannessen, O. M., E. V. Shalina, and M. W. Miles, 1999: Satellite evidence for an Arctic sea ice cover in transformation. *Science*, **286**, 1937–1939.
- Kalnay, E., and Coauthors, 1996: The NCEP/NCAR 40-Year Reanalysis Project. *Bull. Amer. Meteor. Soc.*, **77**, 437–471.
- Köberle, C., and R. Gerdes, 2003: Mechanisms determining the

- variability of Arctic sea ice conditions and export. *J. Climate*, **16**, 2843–2858.
- Kraus, E. B., and J. S. Turner, 1967: A one-dimensional model of the seasonal thermocline: II. The general theory and its consequences. *Tellus*, **19**, 98–106.
- Kwok, R., G. F. Cunningham, and S. S. Pang, 2004: Fram Strait sea ice outflow. *J. Geophys. Res.*, **109**, C01009, doi:10.1029/2003JC001785.
- Laine, V., 2004: Arctic sea ice regional albedo variability and trends, 1982–1998. *J. Geophys. Res.*, **109**, C06027, doi:10.1029/2003JC001818.
- Makshtas, A. P., S. V. Shoutilin, and E. L. Andreas, 2003: Possible dynamic and thermal causes for the recent decrease in sea ice in the Arctic Basin. *J. Geophys. Res.*, **108**, 3232, doi:10.1029/2001JC000878.
- Mantua, N. J., S. R. Hare, Y. Zhang, J. M. Wallace, and R. C. Francis, 1997: A Pacific interdecadal climate oscillation with impacts on salmon production. *Bull. Amer. Meteor. Soc.*, **78**, 1069–1079.
- Maslanik, J. A., M. C. Serrez, and T. Agnew, 1999: On the record reduction in the western Arctic sea-ice cover in 1998. *Geophys. Res. Lett.*, **26**, 1905–1908.
- Moritz, R. E., C. M. Bitz, and E. J. Steig, 2002: Dynamics of recent climate change in the Arctic. *Science*, **297**, 1497–1502.
- Overland, J. E., and R. L. Colony, 1994: Geostrophic drag coefficients for the central Arctic derived from Soviet drifting station data. *Tellus*, **46A**, 75–85.
- Parkinson, C. L., and W. M. Washington, 1979: A large scale numerical model of sea ice. *J. Geophys. Res.*, **84**, 311–337.
- , D. J. Cavalieri, P. Gloersen, H. J. Zwally, and J. C. Comiso, 1999: Arctic sea ice extents, areas, and trends, 1978–1996. *J. Geophys. Res.*, **104**, 20 837–20 856.
- Proshutinsky, A. Y., and M. A. Johnson, 1997: Two circulation regimes of the wind-driven Arctic Ocean. *J. Geophys. Res.*, **102**, 12 493–12 514.
- Rayner, N. A., E. B. Horton, D. E. Parker, C. K. Folland, and R. B. Hackett, 1996: Version 2.2 of the Global Sea-Ice and Sea Surface Temperature Data Set, 1903–1994. Climate Research Tech. Note 74, Hadley Centre for Climate Prediction and Research, 21 pp.
- Rigor, I. G., and J. M. Wallace, 2004: Variations in age of Arctic sea ice and summer sea-ice extent. *Geophys. Res. Lett.*, **31**, L09401, doi:10.1029/2004GL019492.
- , R. Colony, and S. Martin, 2000: Variations in surface air temperature observations in the Arctic, 1979–1997. *J. Climate*, **13**, 896–914.
- , J. M. Wallace, and R. L. Colony, 2002: Response of sea ice to the Arctic Oscillation. *J. Climate*, **15**, 2648–2663.
- Rothrock, D. A., and J. Zhang, 2005: Arctic Ocean sea ice volume: What explains its recent depletion? *J. Geophys. Res.*, **110**, C01002, doi:10.1029/2004JC002282.
- , Y. Yu, and G. A. Maykut, 1999: Thinning of the Arctic sea-ice cover. *Geophys. Res. Lett.*, **26**, 3469–3472.
- , J. Zhang, and Y. Yu, 2003: The Arctic ice thickness anomaly of the 1990s: A consistent view from observations and models. *J. Geophys. Res.*, **108**, 3083, doi:10.1029/2001JC001208.
- Schweiger, A. J., 2004: Changes in seasonal cloud cover over the Arctic seas from satellite and surface observations. *Geophys. Res. Lett.*, **31**, L12207, doi:10.1029/2004GL020067.
- Serreze, M. C., and Coauthors, 2000: Observational evidence of recent change in the northern high-latitude environment. *Climatic Change*, **46**, 159–207.
- , and Coauthors, 2003: A record minimum Arctic sea ice extent and area in 2002. *Geophys. Res. Lett.*, **30**, doi:10.1029/2002GL016406.
- Stroeve, J. C., M. C. Serreze, F. Fetterer, T. Arbetter, W. Meier, J. Maslanik, and K. Knowles, 2005: Tracking the Arctic's shrinking ice cover: Another extreme September minimum in 2004. *Geophys. Res. Lett.*, **32**, L04501, doi:10.1029/2004GL021810.
- Taylor, K. E., D. Williamson, and F. Zwiers, 2000: The sea surface temperature and sea-ice concentration boundary conditions for AMIP II simulations. PCMDI Rep. 60, Program for Climate Model Diagnosis and Intercomparison, Lawrence Livermore National Laboratory, 28 pp. [Available online at <http://www.lmd.jussieu.fr/pcmdi-mirror/pcmdi/pubs/ab60.html>.]
- Thomas, D., 1999: The quality of sea ice velocity estimates. *J. Geophys. Res.*, **104**, 13 627–13 652.
- Thompson, D. W. J., and J. M. Wallace, 1998: The Arctic Oscillation signature in the wintertime geopotential height and temperature fields. *Geophys. Res. Lett.*, **25**, 1297–1300.
- Thorndike, A. S., and R. Colony, 1982: Sea ice motion in response to geostrophic winds. *J. Geophys. Res.*, **87**, 5845–5852.
- Walsh, J. E., W. L. Chapman, and T. L. Shy, 1996: Recent decrease of sea level pressure in the central Arctic. *J. Climate*, **9**, 480–486.
- Wang, X., and J. R. Key, 2003: Recent trends in Arctic surface, cloud, and radiation properties from space. *Science*, **299**, 1725–1728.
- Winton, M., 2000: A reformulated three-layer sea ice model. *J. Atmos. Oceanic Technol.*, **17**, 525–531.
- Yu, Y., G. A. Maykut, and D. A. Rothrock, 2004: Changes in the thickness distribution of Arctic sea ice between 1958–1970 and 1993–1997. *J. Geophys. Res.*, **109**, C05013, doi:10.1029/2003JC002106.
- Zhang, J., and W. D. Hibler III, 1997: On an efficient numerical method for modeling sea ice dynamics. *J. Geophys. Res.*, **102**, 8691–8702.
- , and D. A. Rothrock, 2001: A thickness and enthalpy distribution sea-ice model. *J. Phys. Oceanogr.*, **31**, 2986–3001.
- , W. D. Hibler III, M. Steele, and D. A. Rothrock, 1998: Arctic ice–ocean modeling with and without climate restoring. *J. Phys. Oceanogr.*, **28**, 191–217.
- , D. A. Rothrock, and M. Steele, 2000: Recent changes in Arctic sea ice: The interplay between ice dynamics and thermodynamics. *J. Climate*, **13**, 3099–3114.
- , D. Thomas, D. A. Rothrock, R. W. Lindsay, Y. Yu, and R. Kwok, 2003: Assimilation of ice motion observations and comparisons with submarine ice thickness data. *J. Geophys. Res.*, **108**, 3170, doi:10.1029/2001JC001041.
- , M. Steele, D. A. Rothrock, and R. W. Lindsay, 2004: Increasing exchanges at Greenland–Scotland Ridge and their links with the North Atlantic Oscillation and Arctic sea ice. *Geophys. Res. Lett.*, **31**, L06503, doi:10.1029/2003GL019303.